Provided for non-commercial research and education use.
Not for reproduction, distribution or commercial use.

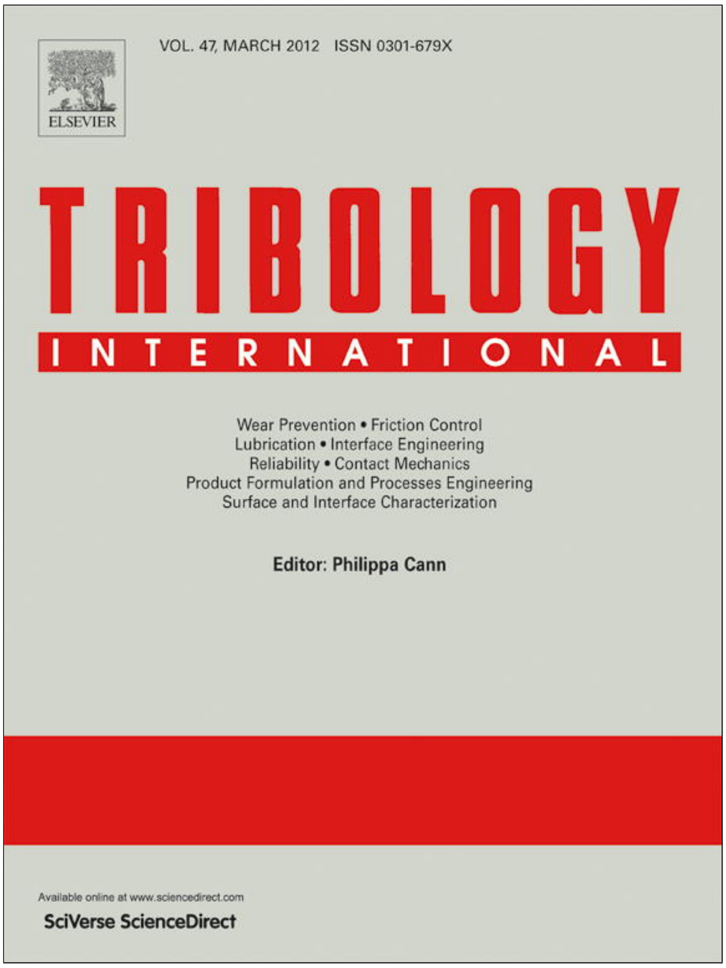

VOL. 47, MARCH 2012 ISSN 0301-679X

ELSEVIER

TRIBOLOGY
INTERNATIONAL

Wear Prevention • Friction Control
Lubrication • Interface Engineering
Reliability • Contact Mechanics
Product Formulation and Processes Engineering
Surface and Interface Characterization

Editor: Philippa Cann

Available online at www.sciencedirect.com
SciVerse ScienceDirect

This article appeared in a journal published by Elsevier. The attached copy is furnished to the author for internal non-commercial research and education use, including for instruction at the authors institution and sharing with colleagues.

Other uses, including reproduction and distribution, or selling or licensing copies, or posting to personal, institutional or third party websites are prohibited.

In most cases authors are permitted to post their version of the article (e.g. in Word or Tex form) to their personal website or institutional repository. Authors requiring further information regarding Elsevier's archiving and manuscript policies are encouraged to visit:

http://www.elsevier.com/copyright

Tribology International 47 (2012) 69–76

Contents lists available at SciVerse ScienceDirect

Tribology International

journal homepage: www.elsevier.com/locate/triboint

Determination of a large tilting pad thrust bearing angular stiffness

D.V. Srikanth [a],*, Kaushal K. Chaturvedi [b], A. Chenna Kesava Reddy [c]

[a] *Mechanical Engineering, Bhaskar Engineering College, Yenkapally, Moinabad, R.R. District, AP, India*
[b] *BHEL (R&D), Vikas Nagar, Hyderabad 500093, AP, India*
[c] *Mechanical Engineering, JNTU Engineering College, Hyderabad, AP, India*

ARTICLE INFO

Article history:
Received 30 May 2011
Received in revised form
24 September 2011
Accepted 18 October 2011
Available online 6 November 2011

Keywords:
Hydrodynamic lubrication
Simulation
Deformation
Bearings

ABSTRACT

A finite difference procedure to solve the Reynolds' and energy equations for the pressure and temperature distribution across the film is described. The film temperature takes viscosity variation and hot oil carryover into consideration. A coupled finite element method using ANSYS determines the important pad deformation. Torques for pad positions 1and 2 are calculated. The angular stiffness pertaining to the 2–1 pair is calculated for 0.5–20% variation of h_o. The values of K_t^* converge asymptotically. The novel interpolation of a single pad's angular stiffness results to determine the characteristics of the bearing are highlighted. Unlike in earlier studies this analysis is helpful in understanding the factors causing pad flutter and dynamics of the bearing elements in hydrogenerators.

© 2011 Elsevier Ltd. All rights reserved.

1. Introduction

Large hydroelectric generators are usually designed as vertical axis machines with the generator above a hydraulic turbine. The rotating parts and hydraulic load are supported by a thrust bearing. To design tilting pad thrust bearings compatible with the given operating conditions, performance characteristics such as load capacity, film thickness, stiffness coefficients, among others are to be determined as in [1]. Investigations on the angular stiffness characteristics of a centrally pivoted-pad oil film for thrust bearings are very scarce to date. The review of literature in [2] shows that there is also a paucity of data related to the oil film of an offset pivot bearing in the fully flooded mode. The purpose of this study is to develop fast computational routines in order to evaluate the angular stiffness of the film. A novel method to find the angular stiffness of a bearing based on the values of only one rectangular pad is formulated. Table 1 lists the geometry, operating conditions and oil properties of the bearing for which the torsional coefficients are being determined. The pad material properties are also listed. The measurement and predictability are key problems to be solved in order to develop good rotor models. To develop better bearing models it is essential to understand the rotor displacement and bearing forces. The object of the design is to ensure and predict equilibrium of the pad taking into account the restoring forces under variation in film thickness. Also the aim and significance of determining the film torsional and axial stiffness of all the pads in the bearing by interpolating the values obtained from one single pad is discussed.

Khonsari [3] emphasized the importance of thermal effects in fluid-film bearings. The contributions made by researchers were reviewed with an extensive literature survey conducted on the thermal effects in hydrodynamic bearings. It was showed that THD problems can be handled accurately and that computerized bearing designs can be performed. Heshmat and Pinkus [4] showed how a correct bearing performance analysis depends on the accuracy of the oil film temperature prediction at the inlet of a thrust pad. The concepts of flow and heat balances were utilized for predicting the temperature of the oil at the inlet. Experiments showed that 70–90% of the heat generated in a thrust pad entered the next pad and the hot lubricant adhered to the runner in the cavitation zone. Procedure and formulae for calculating the inlet temperature of thrust and journal bearings were described. Nanavati and Fadke [5] showed how the oil temperature of an anti friction thrust bearing assembly for a vertical generator is important as the fatigue life depends on it. Using digital computers a finite difference method based thermal analysis across the bearing assembly was presented. The theoretical oil temperature (obtained by the computation method) was compared with the measured values experimentally.

Jeng and Szeri [6] calculated the linear stiffness and damping coefficients of pivoted pads. Both these parameters were strongly influenced by the degree of crowning. To simulate pad deformation under the combined hydrodynamic and thermal loading, spherical crowning was employed. Numerical solutions for the thermo elasto-hydrodynamic lubrication of a tilting pad based on the three-dimensional flow of a lubricant were obtained by Yang

---

* Corresponding author. Tel.: +91 986 666 6659.
E-mail addresses: dvsrikanth1@hotmail.com (D.V. Srikanth), ckaushal49@gmail.com (K.K. Chaturvedi), dr_acreddy@yahoo.com (A.C.K. Reddy).

0301-679X/$ - see front matter © 2011 Elsevier Ltd. All rights reserved.
doi:10.1016/j.triboint.2011.10.017

Nomenclature

a	oil film shape parameter, $(h_o-h_i)/h_o$
a'	new values of 'a' making % change in h_o
b	length of the bearing, m
h_o	oil film thickness at the trailing edge, m
h_i	oil film thickness at leading edge, m
i	index of the node in radial direction
j	index of the node in circumferential direction
m	number of the nodes on the grid in radial direction
n	number of the nodes in circumferential direction coordinate along n-axis
p	pressure in the oil film, Pa
r	radial coordinate, m
r_o	outer radius of bearing, m
B	thrust segment circumferential length, m
C_P	center of pressure
D_i	inner diameter of the thrust bearing, m
D_o	outer diameter of the thrust bearing, m
$E\square$	heat dissipation rate in the oil film, per unit area, W/m^2
G_P	gap between the pads, m
H	non-dimensional film thickness, h/h_o
K_t	angular stiffness in N.m/radian
K_t^*	non dimensional angular stiffness
K^*	non-dimensional dynamic stiffness coefficient
L	radial length of the thrust pad, m
N	angular speed of the runner, rp
P	non-dimensional pressure$=ph^2/\mu U$
$\mathbf{P}$	pressure matrix in Reynolds' equation
R	non-dimensional radius, r/r_o
R_{cp}	radial coordinate of the center of pressure, M
T	lubricant temperature, °C
U, V	velocity along and normal to surface, m/s
W	load on bearing, N
X	x-coordinate of the center of pressure
X_p	pivot distance
Z	number of pads
β	angular extent of the thrust pad
γ	film thickness ratio
μ	viscosity of oil, Pa s
$\overline{\mu}$	non-dimensional viscosity
θ	angle from the leading edge, radian
θ_{cp}	angular location of the center of pressure, radian
ρ	density of oil, kg/m^3
ω	angular speed of the runner, radian/s
Δr	division on the grid along radial direction, m
Δv	volume of an element of the grid, m^3
$\Delta\theta$	angular division of the grid, radian
Δx	differential displacement, m

and Rodkiewicz [7]. For elastic deformation, the pad is idealized as a uniform plate with free boundary so that a conventional finite difference method displacement establishes the coefficient matrix. The generalized Reynolds', film thickness, inlet pressure, the force and momentum balance equations of the pad are solved simultaneously for the pressure distribution. The finite difference method is carried out with the help of a sweeping scheme to obtain the temperature distribution. For the performance of a large thrust bearing, Sinha et al. [8] provided a realistic simulation of the Reynolds' equation when the film thickness is unknown and the center of pressure is known together with the energy and the bending equations. The resultant film shape of the thrust pad is determined by the thermo-elastic analysis. Glavatskih et al. [9] conducted an experimental and theoretical investigation into the effect of oil thermal properties on the functioning of a tilting pad thrust bearing. Poly-a-olefin oil, ester and mineral oil were chosen for the study. They were so chosen because they had the same viscosity grade (ISO VG46) but different heat capacity, viscosity variation with temperature and thermal conductivity values. Experimental results were obtained from an equalizing tilting pad thrust bearing. A three dimensional theoretical TEHD model was used to analyze the oil performance. The active pad displacements due to temperature and pressure fields were determined. The theoretical and experimental data were compared and analyzed in terms of inlet and outlet film thickness, bearing operating temperature and power loss.

Table 1
Thrust bearing geometry and properties.

Description	Quantity
Outer diameter (m)	1.275
Inner diameter (m)	0.75
Number of pads	6
Thickness (mm)	40
Groove width (mm)	84
Number of springs	–
Operating Conditions	
Load (MN)	–
Rotational speed (rads/s)	14.28
Oil pot temperature (°C)	40
Oil Properties	
ISO grade	–
γ (cSt) at 40 °C	73
γ (cSt) at 100 °C	10.7
ρ (g/m) at 15 °C	0.861
Pad Material Properties	
Young's modulus (GPa)	195
Poisson's ratio	0.29
Thermal Properties	
Thermal expansion/°C	12.2 × 10
Thermal conductivity (W/m-K at 10 °C)	42.6
Specific heat (J/kg-K)	473
Heat transfer coefficient for inner surface	6.015e-4
Heat transfer coefficient for outer surface	30e-6

Kurban and Yildrim [10] analyzed the hydrodynamic behavior of thrust bearings by considering different dimensionless system pressure, speed and geometry of the bearing. The elastic load due to elastic deflection was taken into account as the load-bearing characteristics were included. The general behavior of the thrust bearing was analyzed using a proposed neural network predictor. The result gave superior performance for analyzing the behavior of a thrust bearing undergoing elastic deformation. Markin et al. [11] applied a Finite-element method (FEM) modeling to analyze the performance of hydrodynamic tilting-pad thrust bearing assemblies. A three dimensional model of the bearing assembly was used to assess the influence of operating conditions on bearing parameters such as temperature across the pads. The model was first applied and the results were compared with those of experiments carried out on a spherically pivoted-pad. Good correlation was found between the model and experimental results for maximum oil film temperature, pressure distribution and thickness. The effect of different oil types on a spring-supported thrust bearing was analyzed. Application of the model to investigate the same spring-supported pad, with a resilient surface coating, was also discussed.

Li and Qing [12] derived the equations of film thickness, pressure and temperature in thrust bearings with tilting pads. Algebraic expressions were set up for film force and moment applied on the pads. The transient thermo hydrodynamic lubrication performance of the bearings was studied. The decrease of film thickness caused by enhancing load made the film temperature rise gradually. While the load was enhanced gradually the leaning angle of the pad became greater. Dadouche et al. [13] analyzed the performance of a hydrodynamic thrust bearing with eight fixed pads. A comparison between numerical results and experimental data obtained by a thermo-hydrodynamic model was presented. The analysis of the oil supply temperature, applied load, rotational speed on the thrust bearing performance characteristics such as temperature field, minimum film thickness, leakage flow, and power loss were discussed. William et al. [14] optimized pivoting positions in the radial and circumferential directions of tilting pad thrust and radial bearings. Hydrodynamic principles were used in the design of tilting pad bearings utilized in mechanisms carrying shaft thrust or radial loads. Minimum film thickness for a given running condition of velocity, viscosity, temperature, bearing geometry and loading forces was calculated. The minimum fluid film thickness from the pressure distribution in the load-carrying analysis was solved using a simplified Reynolds' equation derived in one-dimension and applied in two dimensions. Jiang et al. [15] analyzed the effects of elastic deformation of pad surface, rotational speed, axial load and oil viscosity grade on tilting pad thrust bearing performance using the model of TEHD lubrication. The film thickness, Reynolds', viscosity–temperature, energy, heat conduction and elastic deformation equations were simultaneously solved. Results showed that the maximum pressure is reduced and the minimum film thickness is decreased when pad deformation is taken into account. The rotational speed has significant effects on film temperature and thickness. The heavier load leads to an increase in the maximum pressure and a decrease in the film thickness. The oil film with higher viscosity grade has a higher load-carrying capacity and consumes much more energy than that of a low viscosity fluid.

2. Reynolds' equation

The following assumptions are made in the analysis:

1. Steady-state conditions exist in the oil film.
2. The lubricant is incompressible.
3. The lubricant is Newtonian.
4. Flow in the convergent wedge is laminar.
5. Pressure and shear effects on the viscosity are negligible.
6. Variation of the specific heat and density with pressure is negligible.
7. Wherever the oil film becomes divergent due to crowning or thermo-elastic distortion, cavitation is taken into account, by making pressure equal to zero, wherever its value is negative.

The analysis of hydrodynamic thrust bearings have been based on the Reynolds' equation for the pressure distribution. With the increase in capacity of computers, numerical models including the influences of viscosity variations along and across the lubricating film have been developed.

The temperature of the runner along its runner surface varies much less than the temperatures in the thrust pad active face. The temperature of the runner varies by less than 1 °C and the temperature along thrust pad rises by 15–20 °C as referred in [16]. Values of viscosity obtained from the temperature field in the oil film are substituted in the Reynolds' equation, to determine the pressure field. In load estimation the pressure 'fitting' at the edges is made more appropriate to suit realistic condition shown in [17].

The Reynolds' equation for a sector-shaped thrust segment for incompressible lubricant, under steady state condition is given in Eq. (1):

$$\frac{\partial}{\partial r}\left[\frac{rh^3}{\mu}\frac{\partial p}{\partial r}\right]+\frac{1}{r}\frac{\partial}{\partial \theta}\left[\frac{h^3}{\mu}\frac{\partial p}{\partial \theta}\right]=6\omega r\frac{\partial h}{\partial \theta}+12r\frac{\partial h}{\partial t} \tag{1}$$

The Reynolds' equation in non-dimensional form is as shown in Eq. (2):

$$2\frac{\partial}{\partial R}\left[\frac{RH^3}{\overline{\mu}}\right]\frac{\partial p}{\partial R}+\frac{2RH^3}{\overline{\mu}}\frac{\partial^2 P}{\partial R^2}+\frac{2}{\beta^2 R}\frac{\partial P}{\partial \overline{\theta}}\frac{\partial}{\partial \theta}\left[\frac{H^3}{\overline{\mu}}\right]+\frac{2}{\beta^2 R}\frac{H^3}{\overline{\mu}}\frac{\partial^2 P}{\partial \overline{\theta}^2}$$
$$=12R\frac{\partial H}{\partial \theta}+24\mathrm{R}\frac{\partial H}{\partial t}\beta \tag{2}$$

As compared to the above form of the equation, better numerical accuracy can be obtained, if all the first derivative terms in the equation are converted into second derivative terms. Adopting this procedure the following Eq. (3) is obtained.

$$\frac{\partial^2}{\partial R^2}\left[\frac{RH^3 p}{\overline{\mu}}\right]+\frac{RH^3}{\overline{\mu}}\frac{\partial^2 P}{\partial R^2}-P\frac{\partial^2}{\partial R^2}\left[\frac{RH^3}{\overline{\mu}}\right]+\frac{1}{R\beta^2}\frac{\partial^2}{\partial \overline{\theta}^2}\left[\frac{H^3 P}{\overline{\mu}}\right]$$
$$+\frac{1}{R\beta^2}\frac{H^3}{\overline{\mu}}\frac{\partial^2 P}{\partial \overline{\theta}^2}-\frac{P}{R\beta^2}\frac{\partial^2}{\partial \overline{\theta}^2}\left[\frac{H^3}{\overline{\mu}}\right]=12R\frac{\partial H}{\partial \theta}+24R\beta V \tag{3}$$

3. Energy equation

Dowson and Hudson in [18] conceptually developed the foundation for thermo-hydrodynamic lubrication. Abdel-latife in [19] and Ashour and El-Butch in [20] fully or partly considered thermo-elastohydrodynamic theories in their study. The generation of heat lowers the effective oil film viscosity and results in the decreased load capacity. The energy equation governs the heat generation and transport of oil. The energy equation for laminar flow and incompressible lubricant is given in Eq. (4) as

$$C_p\rho\left[q_r\frac{\partial T}{\partial r}+q_\theta\frac{1}{r}\frac{\partial T}{\partial \theta}\right]=E\square \tag{4}$$

Further Eqs. (5), (6) and (7) show that

$$q_r=-\frac{h^3}{12\mu}\frac{\partial p}{\partial r} \tag{5}$$

$$q_\theta=\frac{r\omega h}{2}-\frac{h^3}{12\mu}\frac{1}{r}\frac{\partial p}{\partial \theta} \tag{6}$$

$$E\square=\frac{\mu}{h}(\omega r)^2+\frac{h^3}{12\mu}\left[\left(\frac{1}{r}\frac{\partial p}{\partial \theta}\right)^2+\left(\frac{\partial p}{\partial r}\right)^2\right] \tag{7}$$

The Vogelpohl–Cameron equation in [21] given below in Eq. (9) shows the variation of viscosity with temperature. It is an empirical relation with minimum deviation from observed variation of viscosity with temperature. Two viscosity measurements at temperatures $T1=40$ °C and $T2=100$ °C for the oil under consideration are needed to determine the two constants μ_0 and $\boldsymbol{A}$. The value of $\boldsymbol{A}$ is

$$\boldsymbol{A}=(T1+95)(T2+95)\log\left(\frac{\mu_{40}/\mu_{100}}{\boldsymbol{T}2-\boldsymbol{T}1}\right) \tag{8}$$

$$\mu=\mu_0 e^{\boldsymbol{A}/(\boldsymbol{T}+95)} \tag{9}$$

It is incorporated in the iteration process.

4. Hot oil carry-over effect

The lubricant entering the wedge at the inlet edge is heated up to some extent by the hot runner in the inter-pad space. Further this lubricant consists of some oil pre-heated in the preceding pad and some oil from the bath to make up for the oil lost due to side leakage. Thus, the actual inlet temperature in the oil film is at a higher temperature compared to the bulk oil temperature. Ettles' presented the following Eq. (10)

$$T_{out} = T_{\sup} + \Delta T\left(\frac{2-k}{2-2k}\right) \tag{10}$$

where Eq. (11) gives the value of k as

$$k = \frac{T_{in}-T_{\sup p}}{T_{run}-T_{\sup p}} \tag{11}$$

k is assumed in the study to be $=0.83$

$$T_{in} = T_{out}-\Delta T \tag{12}$$

Thus once the temperature of the bulk oil in the housing is known and the temperature rise calculated, the inlet temperature as in Eq. (12), the outlet temperature and the runner temperature can be calculated.

5. Deformation of pad

The element used to mesh the pad thermo-structural deformation model is the hexahedral Solid 226 element. The Solid 226 element has the following structural–thermal capabilities. It has up to twenty nodes with up to five degrees of freedom per node. Structural capabilities are elastic only and include large deflection and stress stiffening.

Its geometry, node locations, and coordinate system are shown in Fig. 1. In both the above two types of elements the units are specified through the EMUNIT command. The nodal loading for these elements depends upon the KEYOPT (1) function value. Nodal forces are input per unit of depth for a plane analysis. The KEYOPT (1) function determines the element DOF set and corresponding force. It is set equal to the sum of the field keys. For example, KEYOPT (1) set to 11 is for a structural–thermal analysis (structural field KEY+thermal field key=1+10).

The torsional stiffness values of the film are calculated based on the obtained pressure profile taking viscosity variations of the lubricant and structural deformation of the pad into consideration. The renewed nodal film thickness is equal to the sum of the original film thickness plus the corresponding nodal deformation.

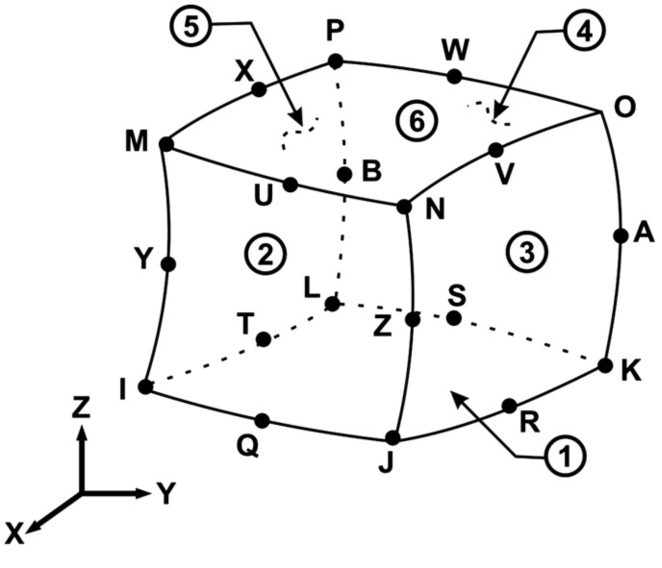

Fig. 1. Solid 226 element geometry.

6. Computational procedure

Solution of the Reynolds' equation using finite difference discretization of the thrust pad is done by considering a total of 81 nodes in the form of a grid as shown in Fig. 2. The Reynolds' equation is a non-homogeneous partial differential equation of two variables for which closed form analytical solutions are not available. The use of finite difference methods for a numerical approximation of this partial differential equation is discussed in [22].

The finite difference equation is derived by approximating the derivatives in the differential equation via the truncated Taylor series expansion for three successive grid points. The central difference from where the values of the function at adjacent nodes on either side are required to evaluate the derivatives is used. Writing the Reynolds' equation in the finite difference form as in Eq. (13) results in a set of linear algebraic equations, which can be transformed into matrix form and solved simultaneously by available subroutines.

This yields the non-dimensional pressure at each node.

$$\begin{aligned}
&P_{i+1,j}\left[\frac{R_{i,j}H_{i,j}^3}{\Delta R^2\overline{\mu}_{i,j}}+\frac{R_{i+1,j}H_{i+1,j}^3}{\overline{\mu}_{i+1,j}\Delta R^2}\right]+P_{i-1,j}\left[\frac{R_{i,j}H_{i,j}^3}{\Delta R^2\overline{\mu}_{i,j}}+\frac{R_{i-1,j}H_{i-1,j}^3}{\overline{\mu}_{i-1,j}\Delta R^2}\right]\\
&\quad+P_{i,j+1}\left[\frac{H_{i,j}^3}{R_{i,j}\overline{\mu}_{i,j}\beta^2\Delta\overline{\theta}^2}+\frac{H_{i,j+1}^3}{R_{i,j}\overline{\mu}_{i,j+1}\beta^2\Delta\overline{\theta}^2}\right]\\
&\quad+P_{i,j-1}\left[\frac{H_{i,j}^3}{R_{i,j}\overline{\mu}_{i,j}\beta^2\Delta\overline{\theta}^2}+\frac{H_{i,j-1}^3}{R_{i,j}\overline{\mu}_{i,j-1}\beta^2\Delta\overline{\theta}^2}\right]\\
&\quad+P_{i,j}\left[-2\frac{R_{i,j}}{\Delta R^2}\frac{H_{i,j}^3}{\overline{\mu}_{i,j}}-\frac{R_{i+1,j}}{\overline{\mu}_{i+1,j}}\frac{H_{i+1,j}^3}{\Delta R^2}-\frac{R_{i-1,j}}{\overline{\mu}_{i-1,j}}\frac{H_{i-1,j}^3}{\Delta R^2}\right.\\
&\quad\left.-2\frac{H_{i,j}^3}{R_{i,j}\overline{\mu}_{i,j}\beta^2\Delta\overline{\theta}^2}-\frac{H_{i,j+1}^3}{R_{i,j}\overline{\mu}_{i,j+1}\beta^2\Delta\overline{\theta}^2}-\frac{H_{i,j-1}^3}{R_{i,j}\overline{\mu}_{i,j-1}\beta^2\Delta\overline{\theta}^2}\right]\\
&=\frac{6R_{i,j}}{\Delta\theta}[H_{i,j+1}-H_{i,j-1}]+12R_{i,j}\beta V
\end{aligned} \tag{13}$$

The calculation procedure uses these pressures along with numerical methods for integration to obtain the load capacity, radial and angular location of center of pressure. Fig. 3 shows the location of the center of pressure on the thrust pad. This yields the non-dimensional pressure at each node.

Solution of the energy equation is also set up in finite differences. The propagation method is used to solve the equation in view of its first order. The initial temperature at the leading edge is specified so that successive values of the downstream temperature are marched out in the flow direction. In this procedure, taking hot oil carry over effect into consideration the temperature distribution is obtained in a single sweep. As the energy Eq. (4) depends upon the pressure gradient, it is solved simultaneously with the Reynolds' equation using the same grid. In the energy equation on incorporating the

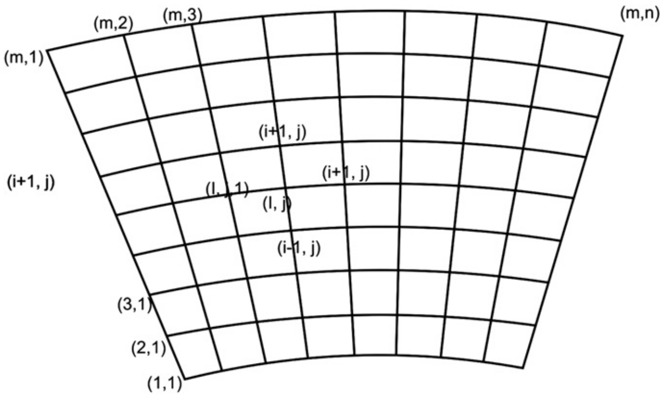

Fig. 2. Discretization of pad for the Reynolds' equation.

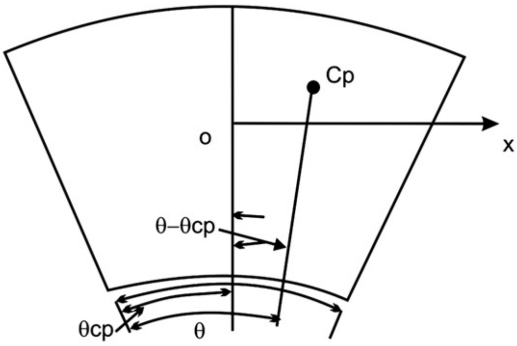

Fig. 3. Thrust pad showing center of pressure.

Vogelpohl–Cameron equation the temperature varies along the flow of the lubricant as shown in Fig. 8. The initial values of uniform temperature and viscosity distribution are used to solve the Reynolds' equation. q_r and q_θ are determined from Eqs. (5) and (6). Eq. (4) is solved for $T(r,\theta)$ and hence $\mu(T)$. Reynolds' equation is then resolved for pressure using the new distribution for viscosity. This iterative scheme converged quickly.

A finite element analysis of the structural and coupled thermo-structural deformation of the thrust pad is done using ANSYS. In pre-processing the cross-sectional geometry, material properties and load data as given in Table 1 are input. The solid model development and the problem meshing is the first step in the analysis. For the solid model creation there are different possibilities. The ANSYS software is used in this case. The problem symmetry should be used to the extent possible so as to decrease the physical dimension and use the smallest mesh-size for the given computer capacity. The model is created in ANSYS using key points in the axis co-ordinate system, joining consecutive lines, creating areas operating and extruding about the axis. After creation the pad model is meshed using the plane 42 and Solid 226 elements for the plane structural and coupled fields, respectively, and simulated.

The pressure and temperature values at the pad bottom surface element nodes are identical to and obtained from the nodal solution of the Reynolds' and energy equations. Inputs in the coupled field analysis apart from the material properties include thermal properties of the material including thermal conductivity, specific heat and density of the material as given in Table 1. For the plane structural deformation case, there are 8 plane 42 elements in the radial and 8 in the circumferential direction to a total of 64 elements in the plane grid. The 3-dimensional size and shape of the plane 42 element grid is visible by switching on the display and the element function.

For the coupled thermo-structural deformation the elemental plot of the pad is displayed in Fig. 4. There are 8 elements in radial, 8 in circumferential and 8 along thickness to a total of 512 hexahedral Solid 226 elements in the deformation function.

Using the axis symmetric boundary condition pressure and corresponding structural load are applied on the area A2 at the bottom surface of pad as per Fig. 5.

(2) The convection from the areas A1, A5, A4 and A6 as shown in Fig. 5 where in the bulk temperature is 40 °C and convection film coefficient value is 4e6 is considered. The area A6 is affected by hot oil carry-over.

(3) The heat flux values for the elemental nodes of the bottom surface of the pad are obtained from the solution of the energy equation.

(4) Radiation heat transfer from the pad is not considered.

To view results for deformation the current load system functions of plot results, counter plot nodal solution and displacement vector are chosen.

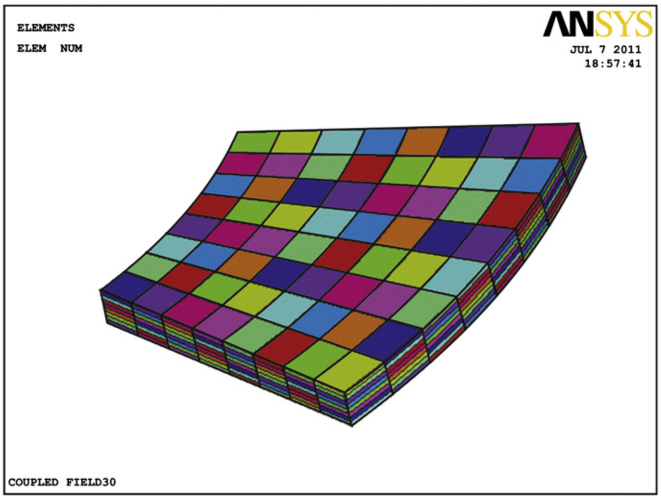

Fig. 4. Elemental plot of the pad.

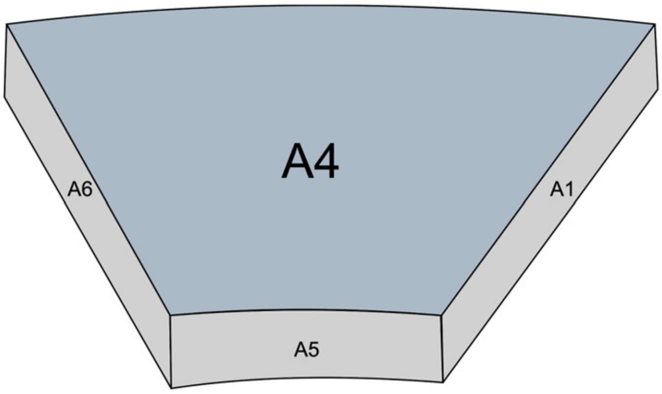

Fig. 5. Areas for applicable loads.

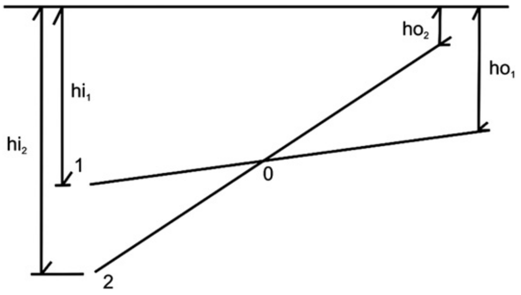

Fig. 6. Pad showing 1, 2 positions for torque calculation.

7. Governing equations

Fig. 6 shows two different pad tilt positions 1 & 2 and corresponding film shapes for which torques are calculated. Referring to Fig. 7 we have the initial value of

$$a=\frac{h_i}{h_o}-1 \tag{14}$$

For the case under consideration the value of h_i is constant and h_o is varied by 20%, 15%, 10%, 7%, 5%, 2%, 1%, 0.5%. The corresponding values of 'a' are calculated using the formula in Eqs. (15) and (16). The mean film thickness at the center of the pad is constant

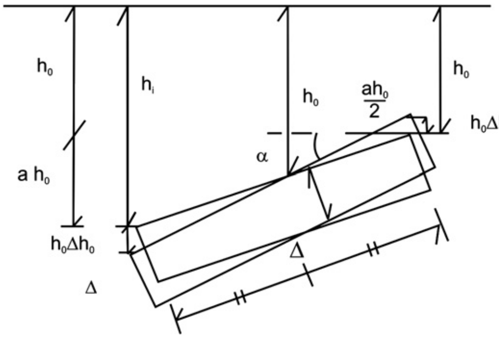
h$_0$
h$_i$
h$_0$
$\frac{ah_0}{2}$
h$_0$
h$_0$Δh$_0$
α
a h$_0$
h$_0$Δh$_0$
Δ
Δ

Fig. 7. Pad showing inlet and outlet film thickness.

so that the load is kept constant

$$a' = \frac{(ah_o + h_o\Delta ho)}{h_o - h_o\Delta ho} \tag{15}$$

$$a' = \frac{(a + \Delta ho)}{1 - \Delta ho} \tag{16}$$

where $\Delta ho = \%$ of h_o increased at leading edge.

The angular stiffnesses of the film pertaining to the 2–1 pair are calculated as follows:

For each variation of h_o, the following values are calculated. X is the x-coordinate of the center of pressure of the film shape under consideration.

$B = R_{cp} \times \text{Beta}$
$X = r\sin(\theta - \theta_{cp})$ to obtain

$$K_T = \frac{W_1 XB}{a(h_{o2} - h_{o1})} \tag{17}$$

Substituting as per Eq. (18) load capacity

$$W^* = \left[\frac{Who^3}{BL^2 U\mu eff}\right] \tag{18}$$

as in [23] in place of W in the following Eq. (19)

$$K_T = \frac{WXB}{ah_o} \tag{19}$$

By rationalizing the non-dimensional angular stiffness K_T^* of the film to a dimensionless number we obtain it in Eq. (20) as

$$K_T^* = K_T\left[\frac{hO^2}{B^2 L^2 U\mu}\right] \tag{20}$$

8. Results and Discussions

To ensure numerical accuracy, the pressure distribution as shown in Fig. 8 satisfies the 0.1% convergence limit. The result for temperature distribution in the oil film for a conventional pad is shown in Fig. 9. The maximum temperature is at the corner of the trailing edge and the outer radius. The temperature contours near the trailing edge and the inner radius is bent forward, which shows less temperature rise. The temperature variation along the left half of the pad is less when compared to the right half.

Fig. 10 below shows the pad indicating the extent of structural-thermal deformation due to pressure and thermal gradient, which amounts to 0.704E-3 mm.

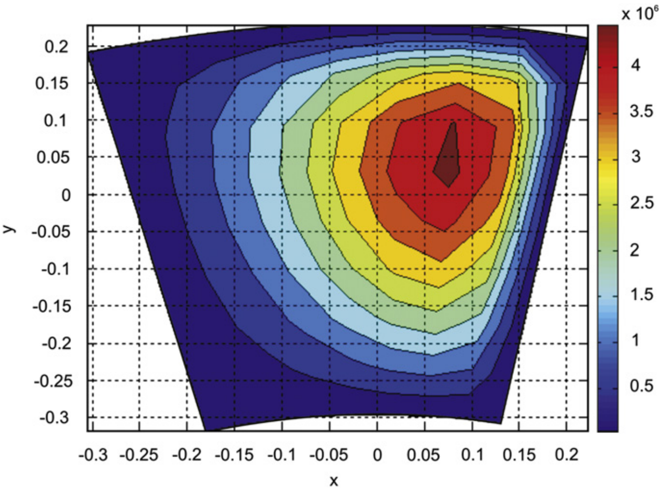

Fig. 8. Pressure distribution in the oil film of a flat pad.

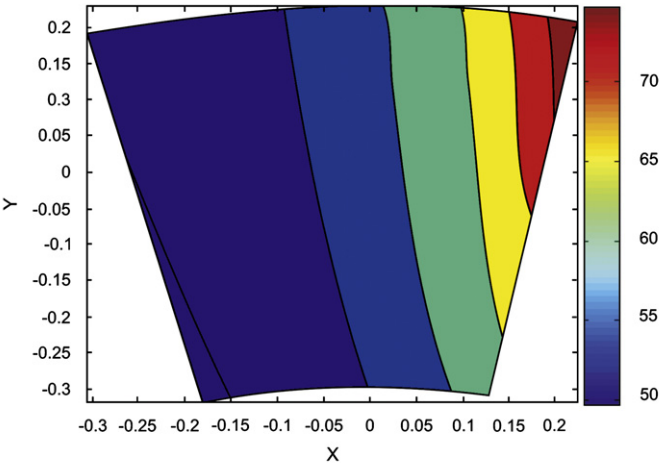

Fig. 9. Temperature distribution in the oil film of pad.

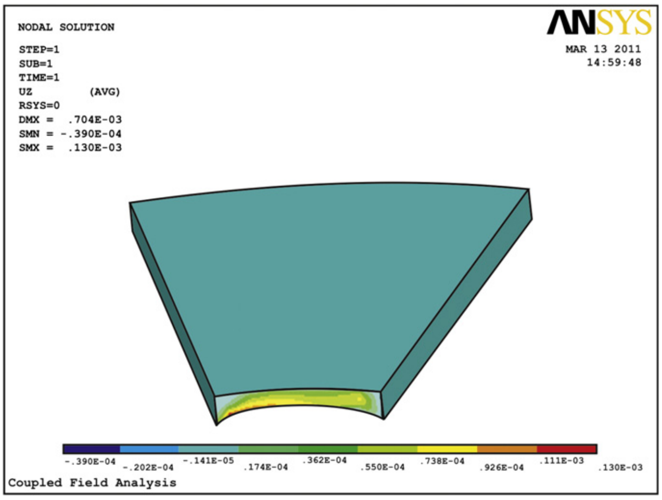
NODAL SOLUTION
STEP=1
SUB=1
TIME=1
UZ (AVG)
RSYS=0
DMX = .704E-03
SMN = -.390E-04
SMX = .130E-03
ANSYS
MAR 13 2011
14:59:48
-.390E-04
-.202E-04
-.141E-05
.174E-04
.362E-04
.550E-04
.738E-04
.926E-04
.111E-03
.130E-03
Coupled Field Analysis

Fig. 10. Pad structural-thermal deformation.

Likewise Fig. 11 shows the plane structural deformation of the pad. For the plane-structural analysis deformation of the pad for the given parameters is equal to 0.726e-3 mm. The renewed film thickness is the sum of the original nodal film thickness plus the corresponding nodal deformation of the pad, which tantamounts to 0.836e-3 mm.

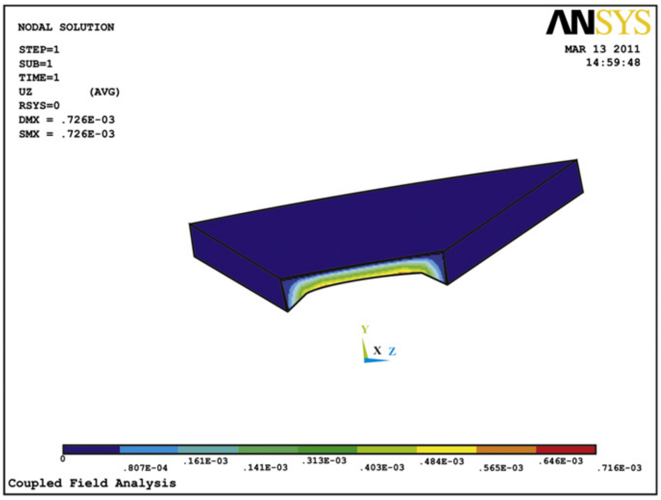

Fig. 11. Front view of pad structural deformation.

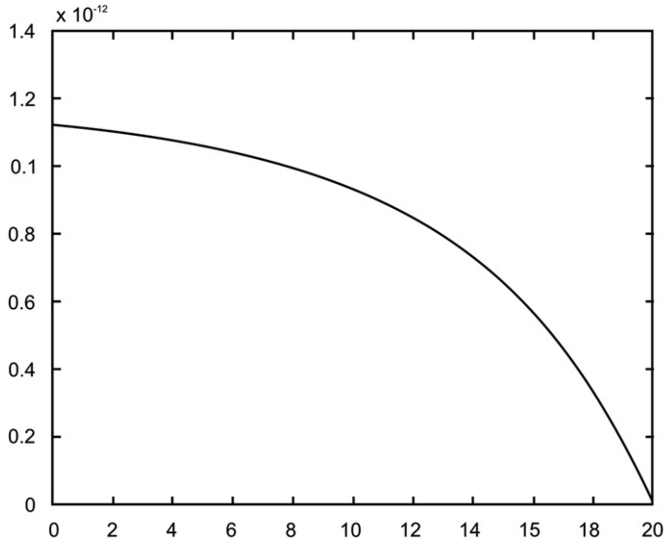

Fig. 12. Percent variation of *ho* vs. dynamic stiffness.

The non dimensional dynamic stiffness K* values are got using Eq. (21) corresponding to % *ho* variation for the 2-1 pair

$$\text{where } K^* = \frac{\Delta W'}{\Delta X}\left[\frac{h_{\min}^3}{BL^2 U\mu eff}\right] \tag{21}$$

Fig. 12 shows the plot where the values of K* tend to converge asymptotically to one value for variation of % h_o. ΔW and Δx values are obtained by taking the difference of W and x values for a particular combination pair and h_o variation.

The significance of Eqs. (16) and (20) lie in the fact that since the non dimensional torsional stiffness of a single pad can be expressed by h_{o1}, h_{o2} and K_T for % variation of h_o from 5 to 20 it is unnecessary to calculate the characteristics of all the pads. When the characteristics of a single pad under a series of parameters h_{o1}, h_{o2} and K_T are obtained the variation is in the form of an asymptotic curve. With an increasing level of perturbation in h_{o1} and h_{o2} in the denominator of Eq. (16) the value of K_T^* decreases and converges at 20% h_o variation. The characteristics of other pads can be calculated by substituting the relevant parameters in the formula.

The torsional stiffness of one pad is recalculated into the axial stiffness of the bearing using Eqs. (19) and (20).

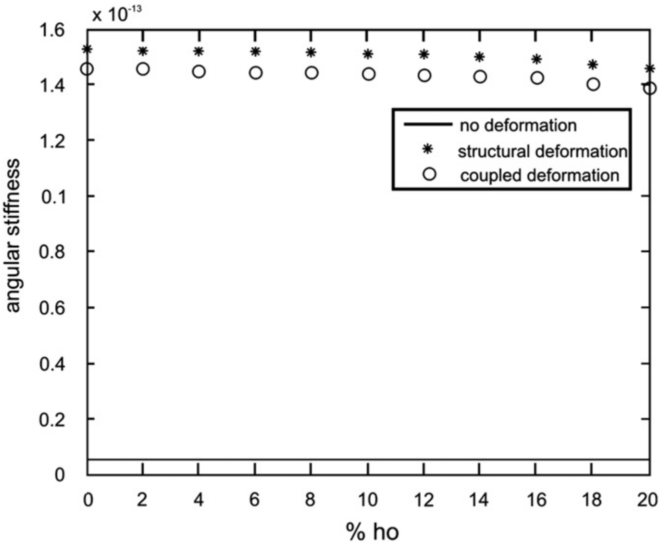

Fig. 13. Non-dimensional angular stiffness variation.

A database for the characteristics of the pads can be developed with help of Eq. (19). The characteristics of all the pads can be obtained by interpolation based on the database. It is unnecessary to solve the perturbed Reynold's equation with respect to pressure and h_{o1}, h_{o2}.

Fig. 13 clearly shows the variation of non dimensional angular stiffness with the type of pad deformation for increasing percentage variation of film thickness. The value of K_t^* converges asymptotically as the % *ho* increases from 0.5 to 20%. There is a big difference in K_T^* values between a pad, which does not take deformation into consideration and one, which takes either plane structural or coupled thermo-structural deformation calculated using the above FEM method. This underlies the importance of pad deformation in large hydro-generator thrust bearings. The difference between angular stiffness values between the two types of deformations considered is not large and the structural deformation produced marginally higher K_T^* values than the coupled field deformation.

9. Conclusions

In order to select thrust bearings compatible with the given operating conditions, first accurate performance characteristics such as bearing metal temperature, load capacity, film thickness, stiffness coefficient among others are to be determined. Two dimensional Reynolds' equation is modified and a finite difference based solution procedure for finding pressure values is written and verified. Numerical integration to these pressure points gives the load. The viscosity variations and corresponding temperature distribution in the transport of the lubricant are taken into consideration for the determination of the film torsional coefficients. The structural deformation of the pad is considered and determined using a three dimensional FEM model using ANSYS. Fast computational routines are developed to evaluate the angular stiffness coefficients taking pad deformation into consideration. Torques and oil film shape parameters, for h_o variation from 0.5 to 20% for 2-1 pair are calculated. The governing equations for angular stiffness pertaining to the 2-1 pair are formulated and verified. The values of K_t^* and K^* converge asymptotically as the % h_o increases from 0.5 to 20%. Also the significance of interpolating the characteristics of all the pads from the torsional coefficients of one pad is discussed. When compared with earlier studies the basic difference is in the dynamic analysis of the oil film, which is subjected to flutter of the thrust segment. In addition to the linear stiffness and damping study as in [24] study of angular stiffness and damping coefficients has been done. This analysis will also be useful for bearings in vertical motor and condensate extract pumps.

References

[1] Hsia-Ming Chu. Shape optimum design of slider bearings using inverse methods. Tribology International 2007;40:906–14.

[2] Jiang PL, Yu L. Rotordynamic modeling of a hydrodynamic pivoted pad thrust bearing. Tribology International 1998;31:175–81.

[3] Khonsari MMA. Review of thermal effects in hydrodynamic bearings Part 1: slider and thrust bearings. ASLE Transactions 1987;30(1):19–25.

[4] Heshmat H, Pinkus O. Mixing inlet temperatures in hydrodynamic bearings. ASME Journal of Tribology 1986;108:231–48.

[5] Nanavati JI, Fadke AS. Determination of oil temperature of a low speed two bearing assembly of vertical machines. Journal of the Institute of Engineering (India) 1994;74:139–43.

[6] Jeng MC, Szeri AZA. Thermo-hydrodynamic solution of pivoted thrust pads: Part III—linearized force coefficients. Transactions of the ASME, Journal of Tribology 1986;108:214–8.

[7] Yang P, Rodkiewicz CM. On the numerical analysis to the thermoelastic hydrodynamic lubrication of a tilting pad thrust bearing inclusive of side leakage. Tribology Transactions 1997;40:259–66.

[8] Sinha AN, Athre K, Biswas S. Non-linear solution of Reynolds equation for thermoelastic hydrodynamic analysis of a thrust pad bearing. Industrial Lubrication and Tribology 2001;53:202–10.

[9] Glavatskih SB, Fillon M, Larsson R. The significance of oil thermal properties on the performance of a tilting pad thrust bearing. ASME, Journal of Tribology 2002;124:377–84.

[10] Kurban AO, Yildrim S. Analysis of a hydrodynamic thrust bearing with elastic deformation using a recurrent neural network. Tribology International 2003;12:943–8.

[11] Markin D, Mc Carthy DMC, Glavatskih SB. A FEM approach to simulation of tilting-pad thrust bearing assemblies. Tribology International 2003;36:807–14.

[12] Li Z, Qing D. Study on transient lubrication performance of thrust bearings with tilting pads set on variation load. Zhongguo Jixie Gongcheng/China Mechanical Engineering 2004;15:1326–8.

[13] Dadouche A, Fillon M, Dmochowski W. Performance of a hydrodynamic fixed geometry thrust bearing comparison between experimental data and numerical results. Tribology Transactions 2006;49:419–26.

[14] William Ni, Christian Griffiths, Bartholme D, Hergert R. Two dimensional analytical analysis of fluid film thickness on pivoted tilting pad bearings. In: Proceedings of the Powertran and Fluid systems conferences and exhibitions. Chicago, IL, USA; 2007 October.

[15] Jiang X, Wang J, Fang J. Thermal elastohydrodynamic lubrication analysis of tilting pad thrust bearings. Proceedings of the IMech, Journal of Engineering Tribology 2011;225:51–7.

[16] Ettles CMM, Anderson HG. Three-dimensional thermo-elastic solutions of thrust bearings using code Marmac 1. ASME Journal of Tribology 1991;112: 405–12.

[17] Chaturvedi KK, Athre K, Nath Y, Biswas S. Refinement in estimation of load capacity and temperature distribution of pad bearing. In: Proceedings of the of Eurotrib-89, 5th international conference on Tribology. Helisinki, Finland; 1989.

[18] Dowson D, Hudson D. Thermo-hydrodynamic analysis of the infinite slider-bearing: Part 1. The plane-inclined slider-bearing. In: Proceedings of the IMechE lubrication and wear convention. 1963, vol. 4, p. 31–41.

[19] Abdel-latife LA. Analysis of heavy loaded tilted pads thrust bearings with large dimensions under TEHD condition. ASME Journal of Tribology 1988;110:407–76.

[20] Ashour NM, El-Butch A. Prediction of the thermal characteristics of thrust bearing with arbitrarily pivoted pad Inter. Colloquium Tribology 2004. (Stuggart-Ostfilerm, Germany).

[21] Stachowiak GW, Batchelor AW. Engineering Tribology. 3rd ed.Elsevier; 2005. p. 13–14.

[22] Capitao JW. Influence of turbulence on performance characteristics of the tilting pad thrust bearing. ASME Journal of Lubrication Technology 1974: 110–7.

[23] Ettles CMM. Some factors affecting the design of spring supported thrust bearings in hydroelectric generators. ASME Journal of Tribology 1991;113: 626–32.

[24] Srikanth DV, Chaturvedi KK, Reddy AC. Modelling of large tilting pad thrust bearing stiffness and damping coefficients. Tribology in Industry 2009;31: 23–8.